Available online at www.sciencedirect.com
SCIENCE DIRECT
Lithos 89 (2006) 47–65
LITHOS
www.elsevier.com/locate/lithos

Geochemical and isotopic constraints on the genesis of the Permian ferropicritic rocks from the Mino–Tamba belt, SW Japan

Yuji Ichiyama [a,*], Akira Ishiwatari [a], Yuka Hirahara [b], Kenji Shuto [c]

[a] Department of Earth Sciences, Faculty of Science, Kanazawa University, Kakuma, Kanazawa, 920-1192, Japan
[b] Graduate School of Science and Technology, Niigata University, 2-8050 Ikarashi, Niigata, 950-2181, Japan
[c] Department of Geology, Faculty of Science, Niigata University, 2-8050 Ikarashi, Niigata, 950-2181, Japan

Received 14 February 2005; accepted 27 September 2005
Available online 14 November 2006

Abstract

The Permian ferropicrite and picritic ferrobasalt occur in the Jurassic accretionary complexes of the Mino–Tamba belt as dikes intruded into the basaltic volcanic rocks. They are characterized by high MgO (11–27 wt.%), FeO* (16–20 wt.%) and HFSE (Nb=24–86 ppm and Zr=103–399 ppm) contents. Mineralogical and petrolographical evidences indicate that their unusual iron-rich nature is apparently magmatic in origin. The incompatible element contents and ratios indicate that the picritic ferrobasalt has close genetic kinship with the previously reported HFSE-rich, but iron-poor picrites, and that they were produced by the low degrees of partial melting of HFSE-enriched source material at high pressures (4–5 GPa). On the other hand, the ferropicrite may have been produced by the same degree of partial melting at a lower pressure, and subsequent olivine accumulation. The Sr and Nd isotopic signatures ($^{87}Sr/^{86}Sr_{(i)}$=0.70266 to 0.70329 and $\varepsilon Nd_{(i)}$=+5.7 to +7.7) of these picritic and ferropicritic rocks are nearly constant and are equivalent to those of HIMU rocks, which require involvement of subducted oceanic crust material into their source region. Nevertheless, the ferropicritic melt cannot have been generated from the iron-poor picrite melt by crystal fractionation. Compared to the compositions of the melts obtained by some melting experiments, production of the unusual ferropicritic melts requires addition of an unreasonable amount of recycled basaltic component into the source mantle peridotite or partial melting at extremely high pressures. A possible source material for the ferropicrite is the mixture of the recycled Fe- and Ti-rich basalt (and/or gabbro) and mantle peridotite. Such a ferrobasalt occurs in the present ocean floor and also in some peridotite massifs as Fe- and Ti-rich eclogite bodies. The ferropicritic magma may have been derived from the Permian, deep mantle plume in an oceanic setting. The occurrence of the ferropicritic rocks and the HFSE-rich, iron-poor picrite in the Mino–Tamba belt implies that the greenstone–limestone–chert complexes in the Mino–Tamba belt may be fragments of an oceanic plateau formed by the Permian superplume activities in paleo-Pacific ocean and subsequently accreted to a continental margin through subduction process in the Jurassic time.

Keywords: Ferropicrite; HIMU magma; Recycled oceanic crust; Permian mantle plume; Mino–Tamba belt; Sr and Nd isotopes

1. Introduction

A ferropicrite is characterized by high-Mg and -Fe (typically FeO*>14 wt.%) content, and was first recognized in the Early Proterozoic Pechenga Group, NW Russia by Hanski and Smolkin (1989). Francis et al.

* Corresponding author. Present address: Society of Gem & Precious Metal, Ohtsu 2094, Kofu, 400-0055, Japan. Tel.: +81 55 243 6147; fax: +81 55 243 6147.
E-mail address: yichi2san@juno.ocn.ne.jp (Y. Ichiyama).

0024-4937/$ - see front matter © 2005 Elsevier B.V. All rights reserved.
doi:10.1016/j.lithos.2005.09.006

(1999) suggested that the occurrences of the iron-rich picritic and komatiitic rocks reflect the high iron content of the Precambrian mantle relative to the present one. Recently, however, Phanerozoic ferropicrites are discovered in some large igneous provinces (LIPs), and it is suggested that the occurrence of ferropicrite is restricted to the LIPs regardless of geologic age, and that the ferropicrite is generated by partial melting of mantle plume consisted of a basalt–peridotite mixture (Gibson et al., 2000; Gibson, 2002).

An accretionary complex commonly consists of the rock sequence composed of mafic volcanics (greenstones), limestone, chert, sandstone and mudstone in younging order, forming the so-called "oceanic plate stratigraphy", which were accreted to a continental margin or an island arc by the long-term subduction of an oceanic plate. Therefore, the investigation of the accreted greenstone provides us indispensable information on the ancient oceanic magmatism before Jurassic. The Mino–Tamba belt is one of the Jurassic accretionary complexes distributed in Japan (Fig. 1). Ichiyama and Ishiwatari (2005) studied the Permian HFSE-rich picrite from the Mino belt, and discussed the genetic relationships with other terrestrial HFSE-rich picrites. They suggested that the HFSE-rich picrites were generated by the partial melting of a mantle plume material containing previously subducted and recycled oceanic crust fragments at polybaric pressures, and that the Mino picrite was derived from the Permian oceanic superplume activity (see also a review by Ishiwatari and Ichiyama, 2004). Recently, we have also found ferropicritic rocks from the Mino–Tamba belt. These rocks have unusually high FeO* content (up to 20 wt.%), and contain iron-rich mineral phases such as aegirine and riebeckite. We believe that these rocks provide important constraint not only on the origin of the Mino–Tamba belt, but also on the Permian igneous activity of the whole earth. In this paper, we report the petrology, mineralogy and geochemistry of the ferropicritic rocks, and discuss their petrogenetic relationship with the Mino HFSE-rich picrite, and other continental and oceanic picrites and their geodynamic implications.

2. Geological outline and mode of occurrence

Geologic structure of the Inner Zone of southwestern Japan is essentially constructed by nappe piles. The Paleozoic–Mesozoic terranes of continental blocks (Hida and Oki), ophiolites (Oeyama and Yakuno), metamorphic belts (Unazuki, Renge, Suo and Ryoke) and accretionary complexes (Akiyoshi, Maizuru, Ultra-Tamba and Mino–Tamba) are tectonically overthrusted in order of increasing age as going upward in the nappe piles (Isozaki and Maruyama, 1991). Analogous structure is also seen in Primorye of Far East Russia, and it is interpreted that the Japanese and Russian nappe piles

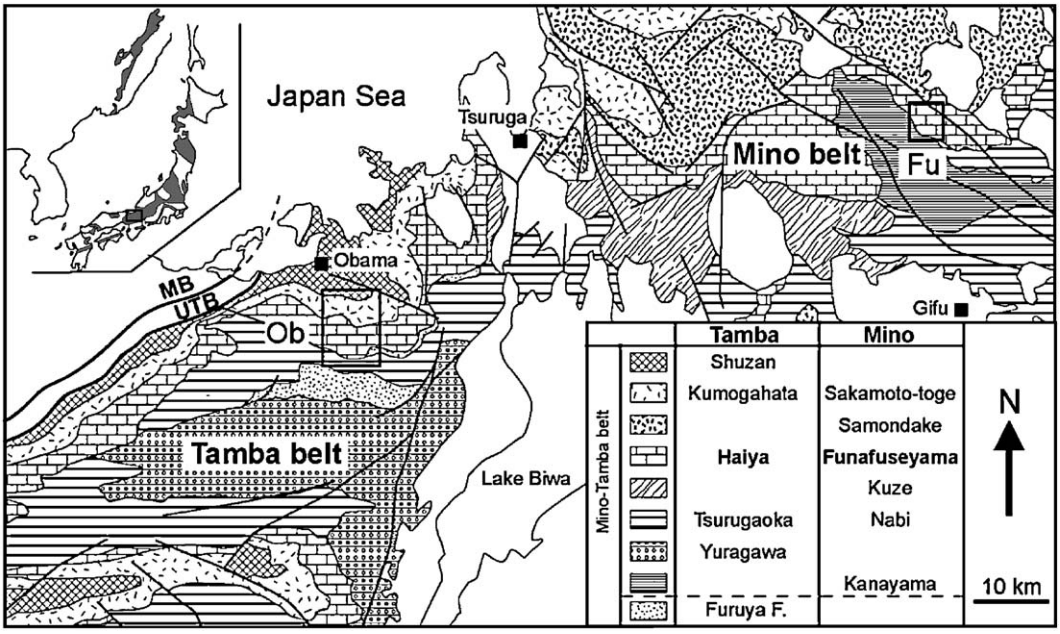

Fig. 1. Distribution of the Jurassic accretionary complexes (gray) in East Asia and geotectonic map of the Mino–Tamba belt in the Inner Zone of southwestern Japan (Nakae, 2000). Ob and Fu indicate the Obama (Tamba) and Funafuseyama (Mino) areas, respectively. UTB and MB indicate the Ultra-Tamba and Maizuru belts, respectively.

were detached from each other by the opening of the Japan Sea during Miocene (e.g. Ishiwatari and Tsujimori, 2003).

The Jurassic accretionary complexes are widely distributed in SW Japan (Fig. 1). It is divided into the Mino and Tamba belts with the boundary at the Lake Biwa. The Mino–Tamba belt is tectonically overthrusted by the Permian Ultra-Tamba belt, and is regionally metamorphosed toward the Median Tectonic Line (Cretaceous low-P/T type Ryoke metamorphic belt). The Mino–Tamba belt also consists of some nappes, and is subdivided into some tectonic units or complexes based on structure, lithology and age (e.g. Wakita, 1988; Isozaki, 1997; Nakae, 2000). The regional classification of complexes has been proposed for each of the Mino and Tamba belts, but Nakae (2000) recently proposes a comprehensive correlation between the complexes in both belts. We follow his proposal (Fig. 1).

The ferropicritic rocks occur in the Obama area of the Tamba belt. In the Obama area, Nakae and Yoshioka (1998) subdivided the Tamba belt into some local complexes named Tada, Shimonegori, Kouchi and Mukugawa and the Late Jurassic Furuya Formation consisted of stratified clastic sequence (Fig. 2). These complexes are equivalent to Shuzan, Kumogahata, Haiya and Tsurugaoka complexes of the type area (Fig. 1), respectively. The ferropicritic rocks occur in the Kouchi (Haiya) complex. This complex is equivalent to the Funafuseyama complex in the Mino belt, where Ichiyama and Ishiwatari (2005) reported the HFSE-rich picrite and basanite sills and related hyaloclastite interbedded with Middle Permian chert at Funafuseyama area (Fig. 1). The Kouchi complex consists of the allochthonous slabs of mafic volcanics, chert, limestone and siliceous mudstone and the mélange composed of the blocks of these rocks in a mudstone matrix. The structurally upper part of the complex is dominated by mélange, whereas the lower part is dominated by the large-scale slabs composed mainly of chert and basaltic rocks. The limestone, chert and mudstone matrix of mélange contain the Early to Middle Permian fusulinids (Isomi and Kuroda, 1958; Sakaguchi et al., 1973), the Late Permian and Early to Middle Jurassic radiolarians, and Middle Jurassic radiolarians (Nakae and Yoshioka, 1998), respectively. Therefore, the age of the mafic volcanic rocks associated with both chert and limestone is Early to Middle Permian. The mafic rocks are basaltic massive and pillow lava, hya-

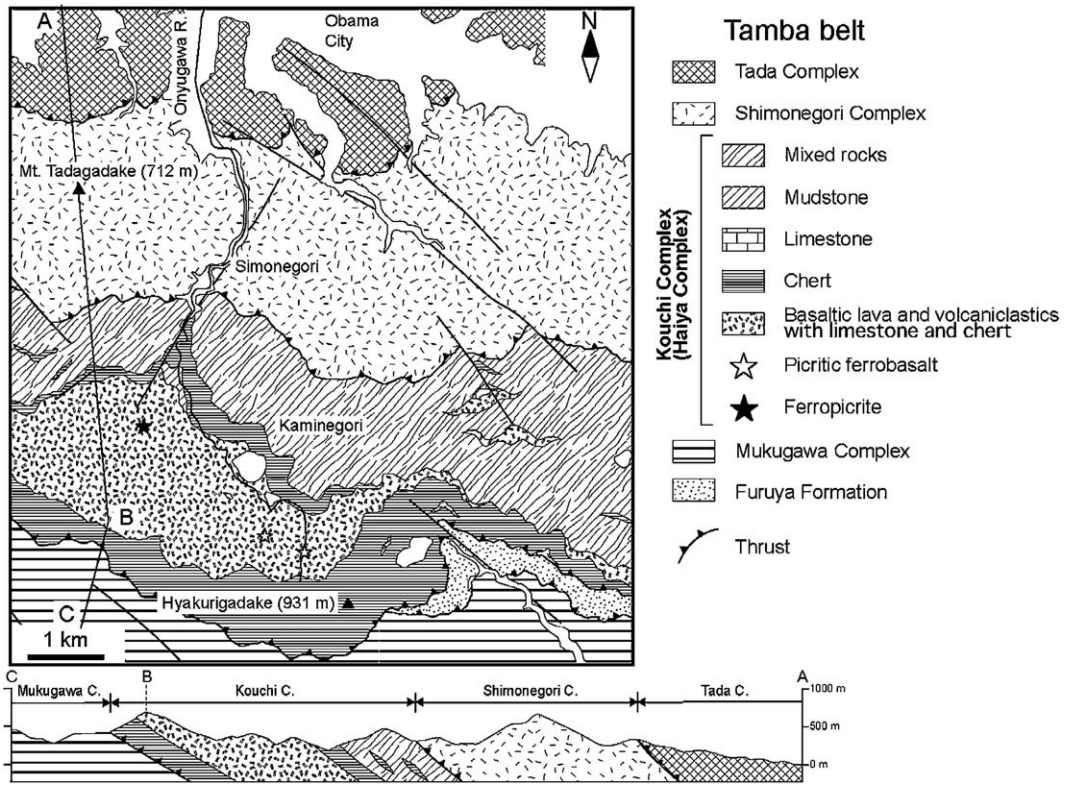

Fig. 2. Geological map of the Obama area in the Tamba belt (Nakae and Yoshioka, 1998) and sampling points of the studied ferropicrite and picritic ferrobasalt.

loclastite and rare dikes, and are associated with chert beds and limestone blocks. The basaltic lava sometimes includes chert xenoliths (up to 30 cm in diameter). Sano and Tazaki (1989) reported the Nd–Sm isochron ages of 303–339 Ma from the mafic volcanics and separated clinopyroxenes in the Tamba belt. However, the error of these ages ranges from ±40 to ±88 Ma, and hence these ages are of low reliability. In this paper, we interpret the age of the mafic rocks as Early Permian (about 280 Ma) based on the fossil record of the overlying chert and limestone as noted above.

The ferropicrite frequently occurs as boulders in a stream of the Ojiga-tani valley, which is a branch of Onyugawa River (Fig. 2). In the upper stream of the Ojiga-tani, the boulders of the aegirine-bearing ankaramite also occur. Judging from the distribution of these boulders, it is likely that the ferropicrite and ankaramite occur as the intrusions (or lava) in basaltic rocks and/or chert. The kaersutite-rich basalt also occurs as a dike intruding into the basaltic rocks. The picritic ferrobasalt occurs as a dike (about 40 m in thickness) associated with an aegirine-bearing gabbro dike intruded into the basaltic lava and hyaloclastite.

3. Analytical techniques

Mineral chemistry was analyzed by a wavelength-dispersive EPMA (JEOL JXA-8800R) at the Cooperative Research Center of Kanazawa University. The analyses were performed under an accelerating voltage of 15 kV and a beam current of 15 nA. JEOL software using ZAF corrections was employed for data reduction. Natural and synthetic minerals of known composition are used as standards. The Fe^{3+} content in the Cr-spinel was estimated by assuming spinel stoichiometry.

Major elements (Si, Ti, Al, Fe, Mn, Mg, Ca, Na, K and P) and trace elements (Ni, Sr, Rb, Ba, Nb, Zr, Y etc.) were analyzed by the Rigaku System 3270 X-ray fluorescence spectrometer with Rh tube at Kanazawa University for fused glass of $Li_2B_4O_7$ (5 g)–rock powder (0.5 g) mixture and pressed pellet of rock powder (5 g), respectively. The analyses were carried out at 50 kV accelerating voltage and 20 mA beam current. Rare earth elements (REE) and some other trace elements (Cr, Ta, Hf, etc.) were determined by instrumental neutron activation analysis (INAA). The INAA samples (0.1 g rock powder) were activated at the Kyoto University Reactor, and analyzed by a Ge (Li) γ-ray detector at the Radioisotope Laboratory for Natural Science and Technology, Kanazawa University. Two rock samples were also analyzed by inductively coupled plasma mass spectrometry using a Thermo Electron X7 at Kanazawa University. The analytical procedure was described by Shirasaka et al. (2004). The consistency between INAA and ICP–MS methods is within about 20% for most elements.

Sr and Nd isotopes of the rock and separated mineral samples were analyzed on a Finnigan MAT262 mass spectrometer at Department of Geology, Niigata University. The analytical procedure follows Miyazaki and Shuto (1998). The analyzed minerals (clinopyroxene and amphibole) were separated using isodynamic separator and heavy liquid (sodium polytungstate). $^{87}Sr/^{86}Sr$ and $^{143}Nd/^{144}Nd$ ratios were normalized to $^{86}Sr/^{88}Sr = 0.1194$ and $^{146}Nd/^{144}Nd = 0.7219$, respectively. During the course of this study, the NBS987 Sr standard gave a mean value of $^{87}Sr/^{86}Sr = 0.7102395 \pm 0.000013$ (n=4) and the JNdi-1 Nd standard gave a mean value of $^{143}Nd/^{144}Nd = 0.512060 \pm 0.000013$ (n=3). Sr, Rb, Nd and Sm contents were also determined by the same methods as isotopes using ^{87}Rb–^{84}Sr and ^{149}Sm–^{150}Nd mixed spikes. Sr and Rb contents of all whole rock samples are determined using XRF, and Nd and Sm contents of some whole rock and separated minerals samples are determined using ICP–MS. εNd was calculated using $(^{143}Nd/^{144}Nd)_{CHUR} = 0.512638$ and $(^{147}Sm/^{144}Nd)_{CHUR} = 0.1967$.

4. Petrography and mineralogy

4.1. Ferropicrite

Representative analyses of the minerals are shown in Table 1. The ferropicrite includes an abundance of olivine (40–45 vol.%) and clinopyroxene (9–11 vol.%) as phenocrysts. The olivine phenocrysts occur as pseudomorphs completely replaced by secondary carbonate, chlorite, talc and serpentinite. It is fine-grained (commonly <1 mm in size) and anhedral to euhedral. Some olivines are poikilitically enclosed by clinopyroxene and amphibole (Fig. 3a). Opaque Cr-spinels are sometimes included in olivine, and are rimmed by magnetite. The Cr-spinels are 66–69 in Cr# (=100Cr/(Cr+Al)), 27–33 in Mg# (=100Mg/(Mg+Fe^{2+})) and 27–30 in Fe^{3+}# (=100Fe^{3+}/(Cr+Al+Fe^{3+})). Some olivines contain spherical, composite inclusions consisting of quenched augite, kaersutite, biotite and magnesioriebeckite (rare) in a chlorite matrix (altered glass) (Fig. 3b and c), which would have been liquid inclusions trapped during the crystallization of the host olivine. The clinopyroxene (<2 mm in size) shows the zoning from yellowish augite in core to pinkish titanaugite in rim. The clinopyroxene phenocrysts are Mg#=82–86, TiO_2=0.8–1.8 wt.% and

Table 1
Representative mineral composition chemistry of the ferropicrite and picritic ferrobasalt from the Obama area, Tamba belt

	Ferropicrite														
Sample	040406-OG1							040522-OG8							
Mineral	Cpx core	Rim	Kaersutite	Biotite	Fe-rich augite	Kaersutite	Riebeckite	Cpx core	Rim	Kaersutite	Biotite	Cr-spinel	Cr-spinel	Kaersutite	Cpx
	Phenocryst		Cpx rim	Groundmasss	Olivine-inclusion			Phenocryst		Cpx rim	Groundmasss	Olivine-inclusion			
SiO_2	50.78	46.43	44.46	37.69	44.15	39.71	52.36	52.16	51.64	41.66	38.69	0.06	0.01	39.71	50.63
TiO_2	1.65	3.74	3.65	5.07	2.60	4.12	0.62	1.17	1.15	5.53	2.89	5.87	5.56	4.12	1.54
Al_2O_3	3.91	7.27	9.65	13.18	8.92	13.53	3.54	2.97	2.93	11.58	12.28	9.95	9.77	13.53	4.46
Cr_2O_3	0.41	0.13	0.00	0.00	0.01	0.03	0.00	0.95	1.00	0.00	0.04	28.73	30.10	0.03	0.00
FeO*	6.12	7.14	9.62	12.46	12.14	14.14	17.48	5.35	5.16	9.32	11.65	45.88	44.04	14.14	7.47
MnO	0.10	0.08	0.13	0.13	0.16	0.22	0.42	0.08	0.11	0.10	0.12	0.42	0.39	0.22	0.19
MgO	15.19	12.81	15.71	18.11	7.95	7.81	13.68	15.88	15.49	14.67	20.66	6.18	6.77	7.81	14.33
CaO	21.90	21.84	10.42	0.00	22.32	16.49	0.76	21.77	21.66	11.35	0.03	0.00	0.00	16.49	21.04
Na_2O	0.45	0.58	3.68	0.11	0.56	1.94	8.79	0.43	0.42	3.20	0.09	0.00	0.00	1.94	0.66
K_2O	0.00	0.00	0.62	8.26	0.00	0.33	0.14	0.01	0.00	0.57	7.46	0.00	0.00	0.33	0.00
Total	100.5	100.02	97.96	95	98.8	98.31	97.79	100.77	99.55	97.99	93.88	97.09	96.65	98.31	100.31
Mg#	0.82	0.76	0.81	0.72	0.54	0.52	0.95	0.84	0.84	0.76	0.76	0.28	0.31	0.52	0.77
Cr#												0.66	0.67		
Fe^{3+}#												0.30	0.29		
An%															

	Picritic ferrobasalt														
Sample	040523-T2								040523-7						
Mineral	Cpx core	Rim	Kaersutite	Aegirine	Biotite	Hornblende	Fe-rich augite	Biotite	Cpx core	Cpx core	Kaersutite	Plagioclase	Biotite	Cpx	Biotite
	Phenocryst		Cpx rim		Groundmasss	Olivine-inclusion			Phenocryst		Cpx rim	Phenocryst	Groundmasss	Olivine-inclusion	
SiO_2	49.32	46.27	40.68	53.37	36.89	42.25	52.42	37.31	47.40	49.61	39.97	57.19	35.37	45.70	33.73
TiO_2	2.04	2.92	3.95	3.41	5.60	1.55	0.21	2.75	2.72	2.10	5.12	0.09	6.51	3.64	2.72
Al_2O_3	4.87	7.16	11.88	1.47	14.89	13.13	3.18	15.08	6.67	4.90	12.93	26.43	15.13	7.75	15.81
Cr_2O_3	0.02	0.01	0.00	0.03	0.01	0.00	0.01	0.00	0.01	0.02	0.04	0.03	0.01	0.01	0.00
FeO*	7.08	7.75	14.69	25.44	13.14	13.99	12.83	15.55	7.90	7.71	12.96	0.63	14.40	8.03	20.18
MnO	0.15	0.15	0.23	0.06	0.10	0.19	0.33	0.13	0.17	0.18	0.25	0.00	0.14	0.12	0.33
MgO	14.01	12.68	11.09	0.27	15.15	12.44	9.44	16.74	12.77	13.74	11.59	0.07	14.14	12.20	14.65
CaO	22.46	21.96	11.23	0.38	0.02	10.91	19.96	0.05	21.37	21.29	11.03	8.45	0.06	21.65	0.06
Na_2O	0.41	0.45	2.95	14.06	0.79	2.81	1.95	0.72	0.48	0.46	2.90	6.01	0.86	0.48	0.28
K_2O	0.02	0.02	1.04	0.05	8.40	0.85	0.03	7.48	0.01	0.00	1.12	0.51	7.79	0.00	4.96
Total	100.37	99.37	97.74	98.53	95.01	98.12	100.36	95.81	99.49	100.01	97.91	99.40	94.39	99.56	92.70
Mg#	0.78	0.74	0.59		0.67	0.74	0.57	0.66	0.74	0.76	0.62		0.64	0.73	0.56
Cr#															
Fe^{3+}#															
An%												0.44			

Al_2O_3 = 1.9–3.9 wt.% in core, while the clinopyroxene in the liquid inclusions are characterized by a more Fe-, Ti- and Al-rich composition (Mg# = 50–63, TiO_2 = 2.1–4.7 wt.% and Al_2O_3 7.1–10.9 wt.%). The clinopyroxene is rimmed by kaersutite, actinolite, cummingtonite and rare magnesioriebeckite. Biotite, apatite and glass (chloritized) fill interstitial spaces. Ilmenite and Ti-magnetite are abundant (up to 4 vol.%). Secondary titanite is also common.

4.2. Picritic ferrobasalt

The picritic ferrobasalt is rich in phenocrysts, which are olivine (about 27–29 vol.%), titanaugite (20–22 vol.%), plagioclase (16–23 vol.%) and rare kaersutite. Olivine phenocrysts are pseudomorphs completely replaced by secondary chlorite and talc. They are fine-grained (<1 mm) and subhedral or euhedral, and are often elongated. Some olivines contain the round-shaped inclusions consisted of augite, kaersutite and biotite in a chlorite matrix. The titanaugite (<1 mm; Mg# = 73–78, TiO_2 = 1.6–3.6 wt.% and Al_2O_3 = 3.7–7.7 wt.% in core) is rimmed by kaersutite and rare aegirine (Fig. 3d). Most plagioclase is replaced by sericite and chlorite, but rare relics are present. Plagioclase ($An_{40–51}$) poikilitically encloses other smaller minerals. The groundmass is composed of altered glass (chlorite), plagioclase, apatite and biotite. The abundant opaque minerals in the groundmass (up to 11 vol.%) are Ti-magnetite and ilmenite. Secondary titanite is also common.

4.3. Other rocks

The ankaramite includes large euhedral titanaugite phenocrysts (up to 3 mm in size; 45 vol.%). The titanaugite (Mg# = 69–80, TiO_2 = 2.1–5.1 wt.% and Al_2O_3 = 5.4–9.6 wt.% in core) is rimmed by green aegirine and aegirine–augite. The interstitial spaces between the large titanaugite phenocrysts are filled with the groundmass composed of smaller grains of titanaugite, aegirine, aegirine–augite, apatite and titanomagnetite and ilmenite. The groundmass also includes altered glass replaced by chlorite and calcite. Minor biotite occurs as accessory minerals. Secondary titanite is common. The kaersutite-rich basalt includes olivine (altered), kaersutite, clinopyroxene (altered) and plagioclase (altered) phenocrysts. The phenocrysts are commonly fine-grained (<1 mm), and kaersutite is the most abundant among them. Apatite and opaque mineral also occur as accessory minerals. The aegirine-bearing gab-

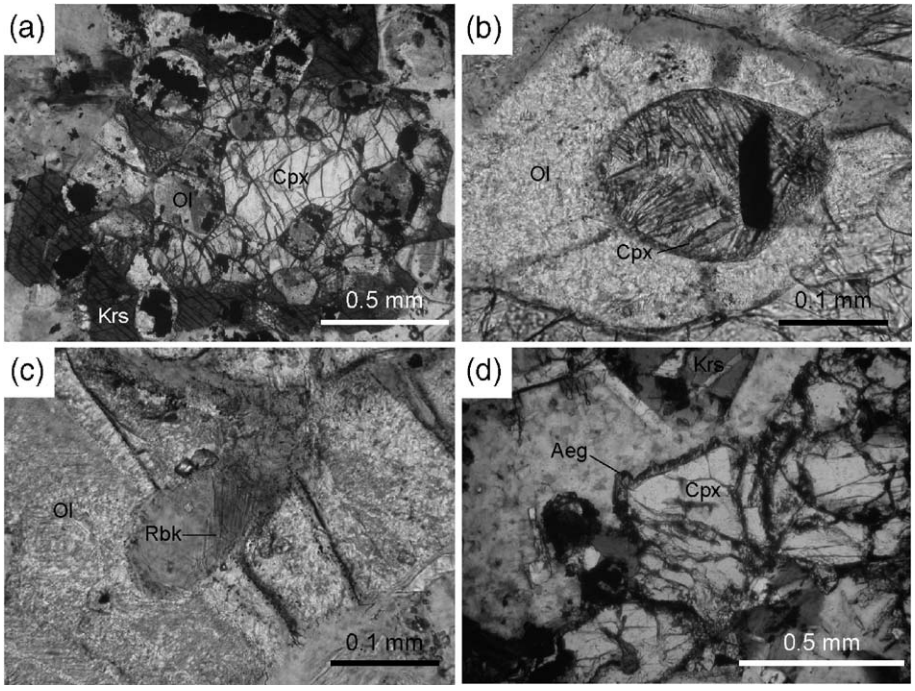

Fig. 3. Photomicrographs of the Tamba ferropicrite (a, b and c) and picritic ferrobasalt (d). All were taken with open nicol. Ol = olivine (pseudomorph), Cpx = clinopyroxene, Krs = kaersutite, Aeg = aegirine and Rbk = riebeckite. (a) Olivine poikilitically enclosed by clinopyroxene with kaersutite rim. (b) Needle-like clinopyroxene in the rounded "melt" inclusion in olivine. (c) Riebeckite in the rounded "melt" inclusion in olivine. (b) Aegirine rimming clinopyroxene.

bro mainly consists of coarse-grained (around 3 mm in size) plagioclase, kaersutite and titanaugite (Mg#=71–76 TiO_2=1.4–2.9 wt.% and Al_2O_3=3.6–6.9 wt.%). The plagioclase is replaced by albite, K-feldspar, chlorite and calcite. Because titanaugite and kaersutite are intensely replaced by chlorite, the estimate of the primary proportion of the two minerals is sometimes difficult. Aegirine, aegirine–augite, apatite, biotite and Fe–Ti oxide occur as accessory minerals. Secondary titanite is also common.

5. Whole rock chemistry

5.1. Major and trace elements

The results of major and trace elements are listed in Table 2. Fig. 4 illustrates the major and trace element compositions with respect to MgO content for the Tamba ferropicrite and picritic ferrobasalt, compared with those of other terrestrial picrites and ferropicrites. The elements mobile during alteration, such as K_2O,

Table 2
Whole rock chemistry of the ferropicrite and picritic ferrobasalt from the Obama area, Tamba belt. FeO* is total iron as FeO

Rock	Ferropicrite				Picritic ferrobasalt			
Sample	040406-OG1	040522-OG8	040605-OG17	040605-OG19	040523-6	040523-7	040523-T2	
SiO_2	45.92	42.00	43.11	44.52	38.66	40.50	38.51	
TiO_2	1.18	1.25	1.30	1.31	4.71	4.34	4.72	
Al_2O_3	5.03	4.60	4.96	5.06	10.12	12.62	10.32	
FeO*	15.13	15.66	16.19	16.79	18.98	15.46	18.60	
MnO	0.16	0.25	0.21	0.14	0.22	0.20	0.22	
MgO	23.75	26.02	23.78	21.64	11.27	10.84	11.33	
CaO	4.41	4.19	5.07	4.97	9.37	9.23	9.19	
Na_2O	0.20	0.39	0.34	0.35	0.90	1.65	0.81	
K_2O	0.09	0.31	0.19	0.07	0.82	0.43	0.88	
P_2O_5	0.32	0.32	0.31	0.34	0.68	0.88	0.69	
Total	96.19	94.99	95.46	95.19	95.73	96.15	95.27	
	XRF	XRF	ICP–MS	XRF	XRF	XRF	XRF	XRF	ICP–MS
Ni	1221	1182	1030	1133	1228	185	132	199	174
Cu	36	25		30	49	30	38	35	
Zn	138	127		126	176	185	164	196	
Pb	1		1.49			2	2		1.33
Rb	5	12	10.0	7	2	26	8	27	22.9
Sr	67	101	87.3	121	95	200	442	174	162
Y	17	16	12.1	17	19	31	36	29	24.7
Zr	103	112	99.2	113	121	317	399	330	315
Nb	24	24	22.3	25	26	65	86	68	66.3
V	105	128	92.0	130	141	518	438	575	366
Ba	75	121	57.2	74	86	463	433	406	284
	INAA	INAA		INAA	INAA	INAA	INAA	INAA	ICP–MS
La	18.3	20.0	17.8	23.3	18.5	43.3	55.6	53.2	48.6
Ce	40.1	38.2	35.1	46.5	38.0	96.7	127	102	101
Nd			17.2		21.1	57.4	69.6	58.3	48.5
Sm	3.49	3.81	3.67	4.36	3.88	9.33	11.8	9.60	9.42
Eu	1.40	1.34	1.23	1.20	1.31	2.61	3.86	3.26	2.94
Gd			3.74						8.82
Tb			0.515						1.13
Dy			2.78						5.85
Yb	1.38	1.58	1.00	1.68	1.64	2.13	3.12	2.34	2.09
Lu		0.142	0.139	0.183	0.216	0.276	0.294	0.265	0.293
Hf	2.31	2.31	2.38	2.98	2.29	6.68	8.27	7.07	7.41
Ta	1.32	1.55	1.58	1.20	1.64	4.54	6.32	4.47	5.19
Th	2.33	2.64	2.08	2.58	2.39	5.02	7.07	5.40	4.89
Cr	932	1219	914	1088	1444	419	289	421	311
Co	122	125	115	120	148	72.6	67.1	81.7	80.2
Sc	13.3	16.1	13.5	15.2	17.0	24.9	20.7	25.0	20.7

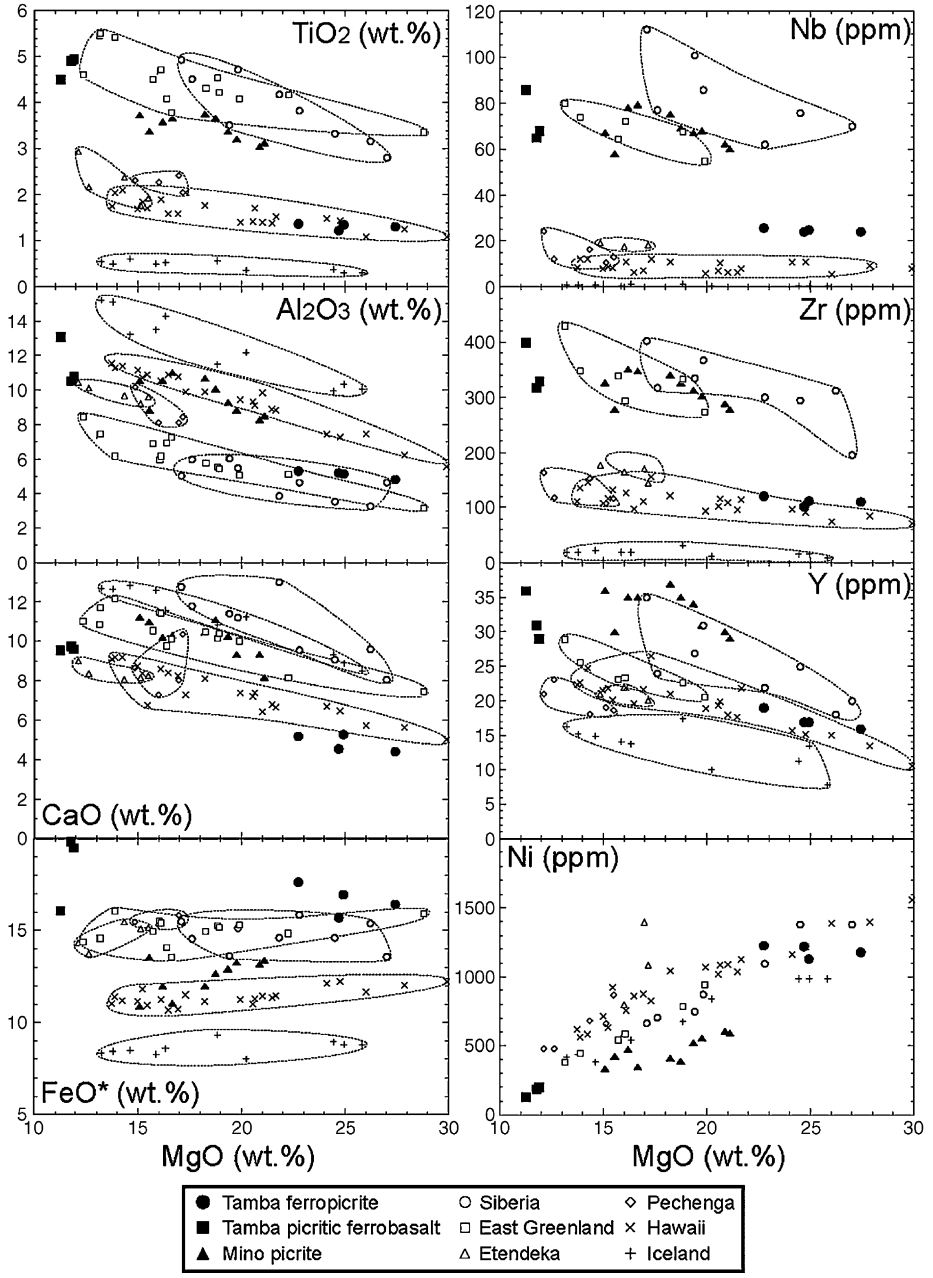

Fig. 4. Major and trace element variations with respect to MgO of the Tamba ferropicrite and picritic ferrobasalt. The plots are recalculated to anhydrous. For comparison, the picrites from the Mino belt (Ichiyama and Ishiwatari, 2005), Iceland (Skovgaard et al., 2001) and Hawaii (Norman and Garcia, 1999) and ferropicrites from Siberia (Arndt et al., 1995), Pechenga (Hanski and Smolkin, 1995), Etendeka (Gibson et al., 2000) and East Greenland (Peate et al., 2003) are also shown.

Na_2O, Ba, Pb and Sr, may have been changed during alteration processes, and in this paper, these elements are not discussed in detail. In general, the major elements such as TiO_2, Al_2O_3 and CaO of the Obama ferropicrite increase with the decrease of MgO content, which is consistent with accumulation or subtraction of olivine. The Tamba ferropicrite is characterized by high MgO (23–27 wt.%) and FeO* (16–18 wt.%) and low TiO_2, (1.2 wt.%), Al_2O_3 (5 wt.%) and CaO (5 wt.%) contents. The picritic ferrobasalt shows lower MgO (around 12 wt.%) and higher FeO* (up to 20 wt.%) than those of the ferropicrite. The TiO_2 (4.5–5.0 wt.%), Al_2O_3 (10–13 wt.%) and P_2O_5 (0.7–0.9 wt.%) contents are significantly high relative to those of the ferropicrite

(TiO_2=1.2–1.3 wt.%, Al_2O_3=4.6–5.1 wt.% and P_2O_5=0.3 wt.%). The FeO* content of the Tamba ferropicrite and picritic ferrobasalt is more than 14 wt.%, and is classified to ferropicrite according to Hanski (1992). This high FeO* content is clearly different from those of common picrites for example from Iceland and Hawaii. In addition, the comparison with the other ferropicrites (Pechenga, Siberia and Etendeka) shows that the Tamba ferropicrite and picritic ferrobasalt contain unusually high FeO* content.

The contents of Nb (24–26 ppm), Zr (103–121 ppm) and Y (16–19 ppm) in the ferropicrite slightly increase with the decrease of MgO, but the Ni content (1130–1230 ppm) does not show clear correlation with MgO. The picritic ferrobasalt is more enriched in Nb (65–86 ppm), Zr (317–399 ppm) and Y (29–36 ppm) and is poorer in Ni (132–199 ppm) than those of the ferropicrite. The trace element patterns of the ferropicrite and picritic ferrobasalt show the similar patterns enriched in more incompatible elements (Fig.

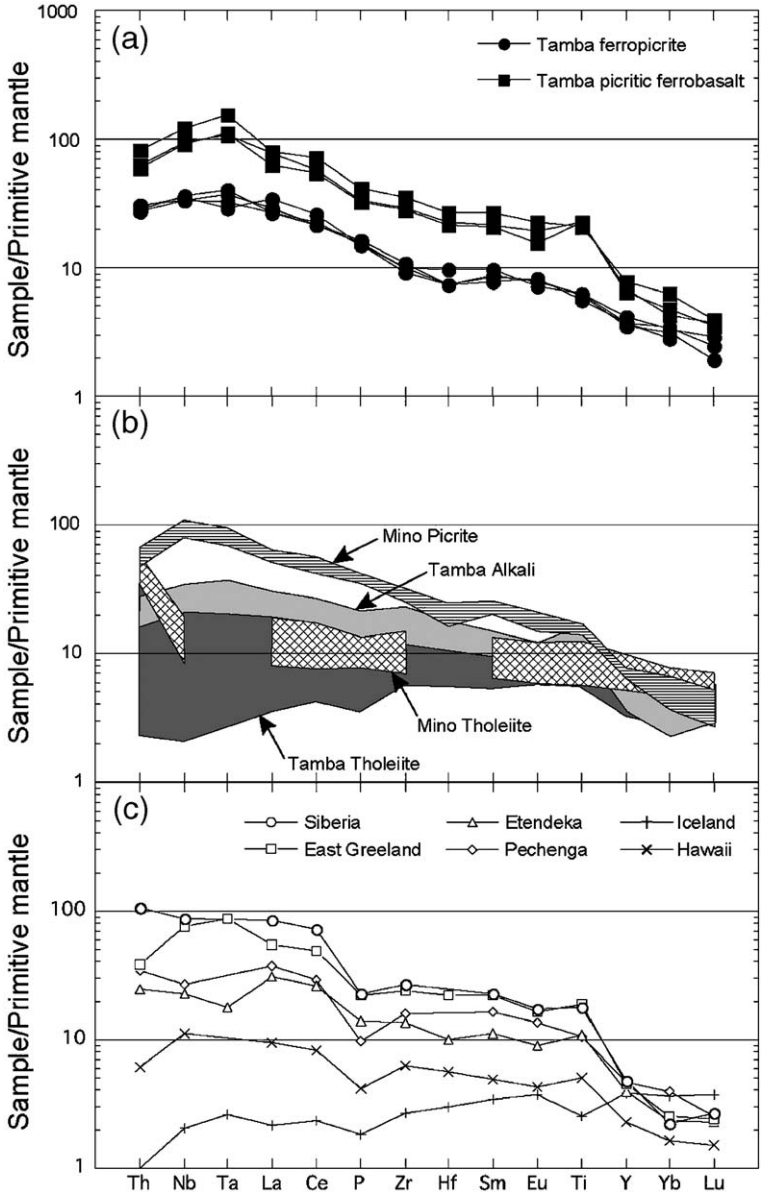

Fig. 5. Primitive mantle-normalized trace element patterns of the Tamba ferropicrite and picritic ferrobasalt (a). For comparison, the patterns of (b) the Mino picrite (Ichiyama and Ishiwatari, 2005), Mino–Tamba basaltic rocks (Tamba tholeiitic and alkali basalts (Sano et al., 2000) and Mino (Funafuseyama) tholeiitic basalts (Jones et al., 1993), and (c) the representative terrestrial picrites and ferropicrites (references are shown in the caption of Fig. 4) are also shown. Primitive mantle values are after Sun and McDonough (1989).

Table 3
Sr and Nd isotopic composition for the picritic rocks from the Mino–Tamba belt

Sample name	Rock	Rb (ppm)	Sr (ppm)	$^{87}Rb/^{86}Sr$	$^{87}Sr/^{86}Sr$	2σ	$^{87}Sr/^{86}Sr_{(i)}$	Sm (ppm)	Nd (ppm)	$^{147}Sm/^{144}Nd$	$^{143}Nd/^{144}Nd_{(i)}$	2σ	$^{143}Nd/^{144}Nd_{(i)}$	εNd
040522-0G8	Ferropicrite	12	101	0.344	0.704028	9	0.702732	3.76	17.6	0.129	0.512867	13	0.512644	6.77
	CPX	0.363	114	0.009	0.702967	14	0.702932	6.43	23.4	0.166	0.512977	14	0.512689	7.66
	CPX+AMP	1.82	275	0.019	0.703364	14	0.703291	10.9	46.4	0.142	0.512883	14	0.512637	6.63
040523-T2	Picritic ferrobasalt	27	174	0.449	0.704356	14	0.702664	*9.42*	*48.5*	0.117	0.512791	19	0.512587	5.67
	CPX	1.98	132	0.043	0.702867	12	0.702703	9.88	37.6	0.159	0.512893	13	0.512617	6.26
	CPX+AMP	12.8	235	0.157	0.703366	14	0.702774	14.5	69.2	0.127	0.512830	14	0.512610	6.12
021117-4L	Mino picrite	7	195	0.104	0.703280	14	0.702888	8.52	39.4	0.131	0.512905	14	0.512678	7.44
	CPX							*8.94*	*29.9*	0.181	0.512962	13	0.512648	6.86
	CPX+AMP	14.6	4074	0.010	0.702769	12	0.702730	*15.6*	*63.5*	0.148	0.512915	11	0.512657	7.04

Italicized numbers represent the value determined by ICP–MS.
Initial value is calculated at 265 Ma.

5). In more detail, the patterns of the picritic ferrobasalt show more depletion of Y and HREE than those of the ferropicrite, and have a slight positive anomaly of Ti. The contents of incompatible element such as Nb, Zr and TiO_2 (HFSEs) in the Tamba ferropicrite are similar to those of the Hawaiian picrite and the Pechenga and Etendeka ferropicrite, although the Nb content is somewhat higher. The contents of these elements in the Tamba picritic ferrobasalt are very high and are similar to those of the Mino picrite and the Siberian ferropicrite. The trace element patterns of the Tamba ferropicrite and picritic ferrobasalt are very enriched in incompatible elements, and also are similar to that of the Mino picrite and Siberian ferropicrite.

5.2. Sr and Nd isotopes

Sr and Nd isotope and Rb, Sr, Nd and Sm contents are listed in Table 3. Fig. 6 shows the initial Sr isotopic ratio ($^{87}Sr/^{86}Sr_{(i)}$) and $\varepsilon Nd_{(i)}$ plots for the whole rock and mineral separations of the ferropicrite and picritic ferrobasalt and the Mino picrite. Initial isotopic ratios are calculated on assumption of the 265 Ma age. This age is based on the hyaloclastite and picrite associated with the Middle Permian chert in the Funafuseyama area, the Mino belt (Ichiyama and Ishiwatari, 2005). The initial Nd isotopic ratios ($^{143}Nd/^{144}Nd_{(i)}$) of these rocks and mineral separations show a nearly constant value (0.51259–0.51269 and $\varepsilon Nd_{(i)}$ = +5.7 to +7.7). On the other hand, their $^{87}Sr/^{86}Sr_{(i)}$ are very low and show

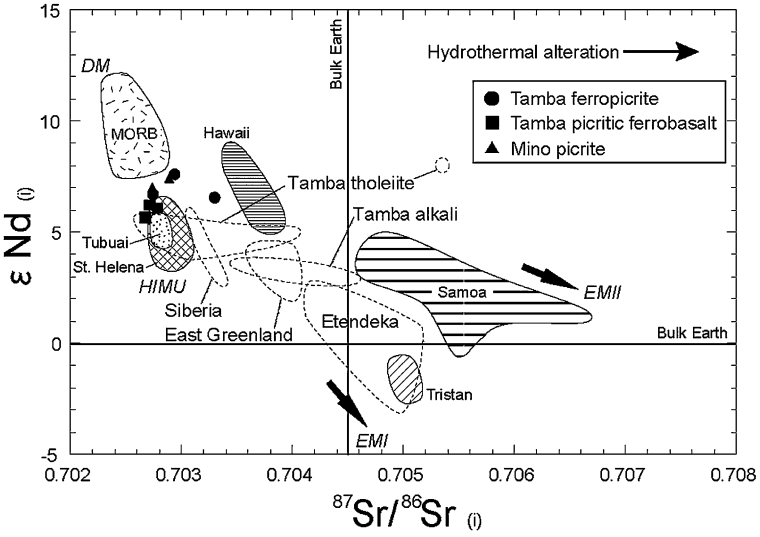

Fig. 6. $^{87}Sr/^{86}Sr_{(i)}$ vs. $\varepsilon Nd_{(i)}$ composition of the Mino–Tamba picritic rocks. The compositional fields of representative volcanic rocks are shown as comparison (East Pacific MORB: White et al., 1987; Hawaii: Stille et al., 1986; Tristan da Cunha: Le Roex et al., 1990; Samoa: Wright and White, 1987; Tubuai: Chauvel et al., 1992; St. Helena: Chaffey et al., 1989). The tholeiitic and alkalic basalts are after Sano and Tazaki (1989). The ferropicrites from Siberia, East Greenland and Etendeka are from the same references as in Fig. 4.

some scattering (0.70266 to 0.70329). In particular, the $^{87}Sr/^{86}Sr_{(i)}$ of the ferropicrites show relatively wide range, which may have resulted from secondary alteration. Because the $^{87}Sr/^{86}Sr_{(i)}$ of the mineral separations of the ferropicrite must be nearer to the original value, the original $^{87}Sr/^{86}Sr_{(i)}$ of the ferropicrite would have been high relative to the other rocks. As a whole, the Sr and Nd isotopic ratios show slightly depleted composition, and are plotted near the fields of MORB (DM) and HIMU (high μ).

6. Discussion

6.1. Iron-rich primary magma

To evaluate the MgO and FeO* contents in igneous stage before alteration, the analyzed contents of the ferropicrite (040406-OG1) and picritic ferrobasalt (040523-7) were compared with the result of simple mass balance calculation. The parameters used in this calculation are the approximate modal and chemical compositions of the minerals in the two rocks (Table 4). The olivine compositions were estimated from the coexisting clinopyroxene compositions, assuming that the Mg–Fe exchange between olivine and clinopyroxene is about 1:1 at high temperature (Loucks, 1996). The MgO content of glass was from the approximate melt compositions saturated in olivine+clinopyroxene and olivine+clinopyroxene+plagioclase, respectively, which are identified by the experimental study at low pressures (Sack et al., 1987). The FeO* content of glass was estimated by assumption of the equilibration with olivine ($(Fe/Mg)^{Ol}/(Fe/Mg)^{liq}=0.3$; Roeder and Emslie, 1970). The results (Table 4) are MgO=21.9 and FeO*=15.0 wt.% in the ferropicrite and MgO=14.2 and FeO*=14.8 wt.% in the picritic ferrobasalt, and indicate the compositional consistency with analyzed MgO and FeO* contents within the range of the modal error and compositional uncertainty.

Cr-spinel is the first liquidus phase crystallizing from a cooling basaltic magma, and its composition is a good indicator of the primary magmas characterizing each tectonic setting (Arai, 1992). In Fig. 7, the compositions of Cr-spinel in the Tamba ferropicrite are shown with the available data of the terrestrial picrites and ferropicrites. The TiO_2 content and Fe^{3+}# of the Tamba ferropicrite are significantly higher than those of MORB (commonly <1 wt.% in TiO_2 and Fe^{3+}# <10), and indicate the affinity with intra-plate basalts (Arai, 1992). These values are also clearly distinguished from those of Hawaii and Iceland. The Cr-spinel of the Tamba ferropicrite is higher in Cr# and Fe^{3+}# and lower in Mg# than those of the HFSE-rich Mino picrite. The spinel compositions of the ferropicrites from Pechenga, Etendeka, Siberia and Tamba show wide scattering, but clearly indicate iron-rich characteristics such as higher Fe^{3+}# and lower Mg# than those of Hawaii and Iceland picrites, which reflect the iron-rich nature of their host rocks.

Ishida et al. (1990) reported the iron-rich picrite (22 wt.% in FeO*) highly sheared during the greenschist–facies metamorphism, and thought that iron content of this rock may have been increased through metamorphism or later alteration. The mass balance calculation and the presence of iron-rich Cr-spinel and clinopyroxene inclusions in olivine phenocrysts indicate that the iron-rich nature of the Tamba ferropicritic rocks was inherited from iron-rich primary magma, not due to the enrichment of iron during secondary alteration. The ferropicrites underwent metamorphism lower than greenschist–facies grade, and contain aegirine and riebeckite (Fig. 3). These minerals appear in high P/T metamorphic rocks and differentiated alkaline igneous rocks such as syenite. Although it is difficult to discriminate whether the aegirine and riebeckite are the products of either during igneous or metamorphic stage, their occurrence is consistent with the iron-rich characteristics of the ferropicrite.

6.2. Compositional differences among the ferropicrites

As shown in Figs. 4 and 5, there are compositional differences, especially in HFSE, among the terrestrial

Table 4
Mass balance calculation for the ferropicrite and picritic ferrobasalt

		Ol	Cpx	Pl	Kaer	Bt	Opq	Gl	Total	Analyzed value
Ferropicrite	Mode (vol.%)	42	12	0	5	3	3	35		
(040406-OG1)	MgO (wt.%)	40.0	14.0	0.0	15.0	18.0	0.0	6.0	21.9	24.7
	FeO* (wt.%)	20.0	7.0	0.0	10.0	10.0	50.0	10.0	15.0	15.7
Picritic ferrobasalt	Mode (vol.%)	27	20	23	5	1	11	13		
(040523-7)	MgO (wt.%)	38.0	13.5	0.0	11.5	15.0	0.0	4.0	14.2	11.3
	FeO* (wt.%)	22.0	8.0	0.0	13.0	14.0	50.0	7.5	14.8	16.1

See text for detail procedure. Ol=olivine, Cpx=clinopyroxene, Pl=plagioclase, Kaer=kaersutite, Bt=biotite, Opq=opaque minerals, Gl=glass.

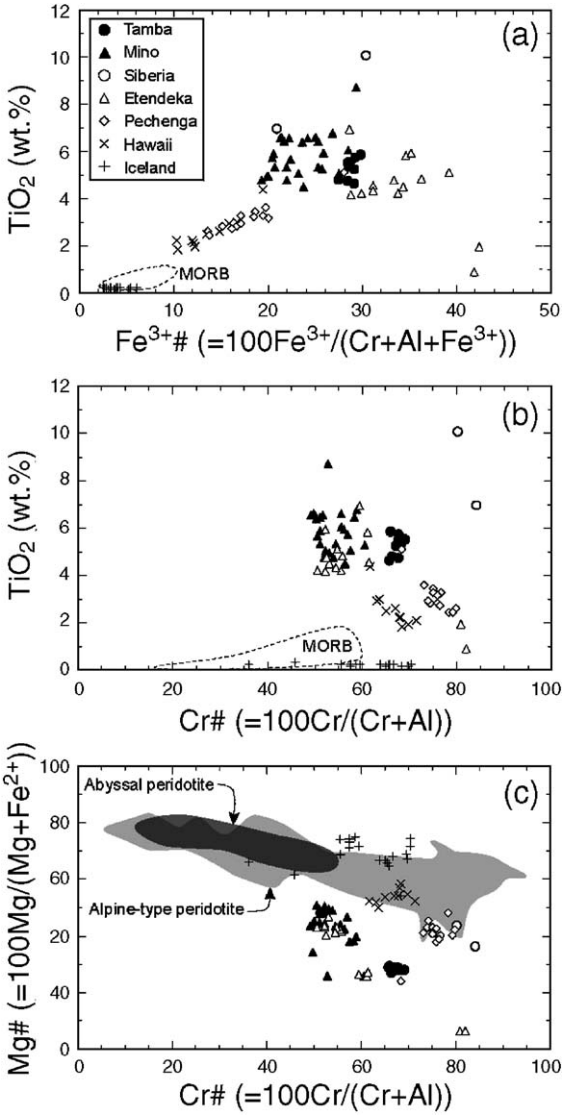

Fig. 7. Cr-spinel compositions of the Tamba ferropicrite and Mino picrite (Ichiyama and Ishiwatari, 2005; Ichiyama, unpublished data). Those of the picrites from Iceland (Sigurdsson et al., 2000) and Hawaii (Nicholls and Stout, 1988) and the ferropicrites from Siberia (Arndt et al., 1995), Etendeka (Gibson et al., 2000) and Pechenga (Hanski, 1992) are also shown. The fields of MORB are after Arai (1992). The compositional fields of the spinel in abyssal and alpine-type peridotites are after Dick and Bullen (1984).

ferropicrites. Although all ferropicrites are enriched in HFSE, the ferropicrites from Siberia, East Greenland and Tamba are significantly enriched in HFSE relative to those of Etendeka and Pechenga. Fig. 8 shows Nb/Zr ratio and Zr content of the Tamba ferropicritic rocks and the terrestrial ferropicrite. Two curves indicate the calculated compositional path of the two melts produced by the batch melting of the primitive peridotite mantle and the mixed mantle at peridotite/MORB (eclogite)=2:1 ratio, respectively. In this diagram, Zr content is changed by variable degrees of olivine accumulation or subtraction, while Nb/Zr ratio is not affected by this process. The ferropicrites are divided into low Nb/Zr ratio (Etendeka and Pechenga) and high Nb/Zr ratio (Tamba, Siberia and East Greenland) groups, suggesting different degrees of partial melting. If these ferropicrites contain no accumulated olivine, the Tamba picritic ferrobasalt and the ferropicrites from Siberia and East Greenland cannot be produced by the partial melting of primitive peridotite mantle due to their too high Zr content. Although it is highly dependant on the selection of the composition and proportion of the source material, any enriched component such as subducted oceanic crust may be necessary in the source region of these picritic magmas. Fig. 9 shows the correlation of Zr/Y and TiO_2/Al_2O_3 ratio, where both ratios increase with the increasing melting pressure (melt segregation depth) due to decrease of Al_2O_3 in clinopyroxene and the increasing stability of garnet in residue with increasing pressure (e.g. Walter, 1998). The Siberian and East Greenland ferropicrites clearly show higher Zr/Y and TiO_2/Al_2O_3 ratios than those of Pechenga and Etendeka, suggesting that the partial melting of the former took place at greater depth relative to the latter. The Tamba ferropicritic rocks show the ratios intermediate between these two groups, but the melting pressure may have been closer to that of the Pechenga and Etendeka ferropicrites.

With respect to isotopic ratios (Fig. 6), the Etendeka and East Greenland ferropicrite extend from HIMU to EMI component, while the Siberian ferropicrite are characterized by low $^{87}Sr/^{86}Sr_{(i)}$ and intermediate $\varepsilon Nd_{(i)}$, which is similar to HIMU and the Mino–Tamba rocks, although the former is slightly higher in $^{87}Sr/^{86}Sr_{(i)}$ and lower in $\epsilon Nd_{(i)}$ values than the Mino–Tamba rocks. Although not plotted, the $\epsilon Nd_{(i)}$ value of +1.4 is reported for the Pechenga ferropicrite by Hanski et al. (1990).

6.3. Relationship among the Tamba ferropicrite, Tamba picritic ferrobasalt and Mino picrite

In $^{87}Sr/^{86}Sr_{(i)}$ and $\varepsilon Nd_{(i)}$ diagram (Fig. 6), the Tamba ferropicritic rocks and Mino picrite are plotted in the same space, suggesting that they are derived from the source material with a similar composition. In addition, these rocks show nearly constant Nb/Zr ratios (Fig. 8), which suggest that they formed by the same degree of partial melting. Their different Zr contents may have resulted from olivine fractionation, but they never share a common parent magma composition because any

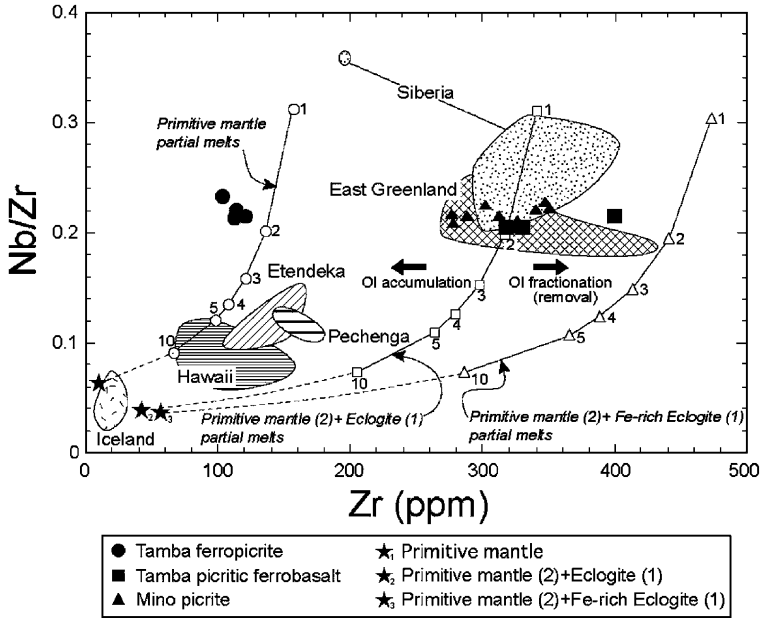

Fig. 8. Nb/Zr ratio vs. Zr content diagram for the Tamba ferropicrite and picritic ferrobasalt. The representative terrestrial picrites and ferropicrites (references are shown in the caption of Fig. 4) are also shown. The paths of calculated partial melts for primitive mantle, primitive mantle+eclogite and primitive mantle+Fe-rich eclogite are also shown. The partial melts are calculated by modal batch melting equation of Shaw (1970). Partition coefficients are after Halliday et al. (1995). The mineral proportion is olivine/orthopyroxene/clinopyroxene/garnet=0.55:0.25:0.15:0.05 in primitive mantle and clinopyroxene/garnet=0.5:0.5 in eclogite. The primitive mantle+eclogite is a mixture of 2:1. The composition of primitive mantle and eclogite (basalt) are after Hofmann (1988). The composition of Fe-rich eclogite is taken from the average composition of Fe-rich basaltic glasses after Regelous et al. (1999). The small numbers near the paths indicate degree of partial melting.

olivine control line cannot connect the ferropicrite and picritic ferrobasalt (Fig. 4). The two picritic ferrobasalts are higher in TiO_2/Al_2O_3 ratio than the other in spite of the same Zr/Y ratio, which corresponds to the Ti positive anomalies in Fig. 5. The Zr/Y and TiO_2/Al_2O_3 ratios of the sample without positive anomaly of Ti are similar to those of the Mino picrite. This leads to the context that the Tamba picritic ferrobasalt formed by the melting of source material at the same pressure as the Mino picrite, which is 4–5 GPa estimated by

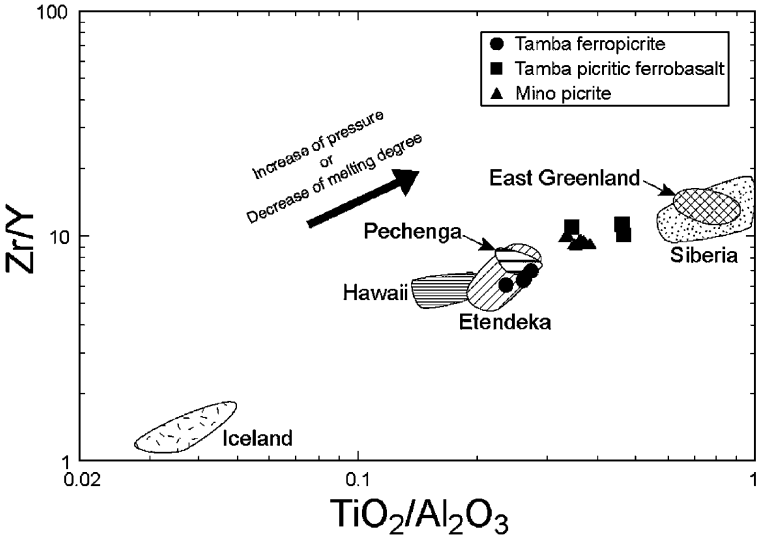

Fig. 9. TiO_2/Al_2O_3 vs. Zr/Y for the Tamba ferropicrite and picritic ferrobasalt. The representative terrestrial picrites and ferropicrites (references are shown in the caption of Fig. 4) are also shown.

Ichiyama and Ishiwatari (2005). In contrast to this, these ratios of the ferropicrite are less than those of the Mino picrite. This is consistent with the absence of the significant fractionation of HREE in the trace element patterns of the ferropicrite, which indicates that the ferropicrite formed by the small degree of partial melting of the similar source material as for the picritic ferrobasalt at shallower depth.

It is likely that the elemental and isotopic relationships between the Tamba picritic ferrobasalt and Mino picrite indicate their strong genetic connection; that is, they were produced by the same degree of partial melting of a common source material at the same depth. Therefore, the more magnesian Mino picrite can be a candidate of parental magma for the Tamba picritic ferrobasalt. To explain the daughter–parent relationship between the picritic ferrobasalt and the Mino picrite, the crystal fractionation of olivine+plagioclase, which is a crystal fractionation sequence observed in MORB or some tholeiitic layered complex (e.g. Mull), might be the most reasonable mechanism to abruptly increase FeO* content in the magma (Fig. 10). However, there is no such possibility of simultaneous crystallization of olivine and plagioclase, because plagioclase is very rare in the Mino picrite (Ichiyama and Ishiwatari, 2005), and plagioclase in the picritic ferrobasalt occurs as poikilitic crystals including all other mineral phases, indicating that it would have been the latest phase during crystallization. Therefore, we get into a dilemma that the Mino picrite shows the same genetic condition as the Tamba picritic ferrobasalt, but they cannot be related as a parent/daughter pair through crystal fractionation.

6.4. Origin of the ferropicrite in the Mino-Tamba belt

The relatively low $^{87}Sr/^{86}Sr_{(i)}$ and high $\varepsilon Nd_{(i)}$ of the Tamba ferropicritic rocks and Mino picrite indicate the source composition similar to MORB or HIMU mantle reservoirs, although a little EM components would have been mixed with their source (particularly ferropicrite, which has relatively high $^{87}Sr/^{86}Sr_{(i)}$). Considering their high concentration of incompatible trace elements and high Nb/Zr ratio, their source material is equivalent to the HIMU mantle source. The HIMU-type volcanic rocks typically appear in Polynesia (e.g. Tubuai Island) and St. Helena (Chauvel et al., 1992; Chaffey et al., 1989), and it has been proposed that its source material is the ancient subducted oceanic lithosphere (e.g. Zindler and Hart, 1986; Weaver, 1991; Chauvel et al., 1992). Among the available isotopic data of the terrestrial ferropicrites, the Siberian ferro-

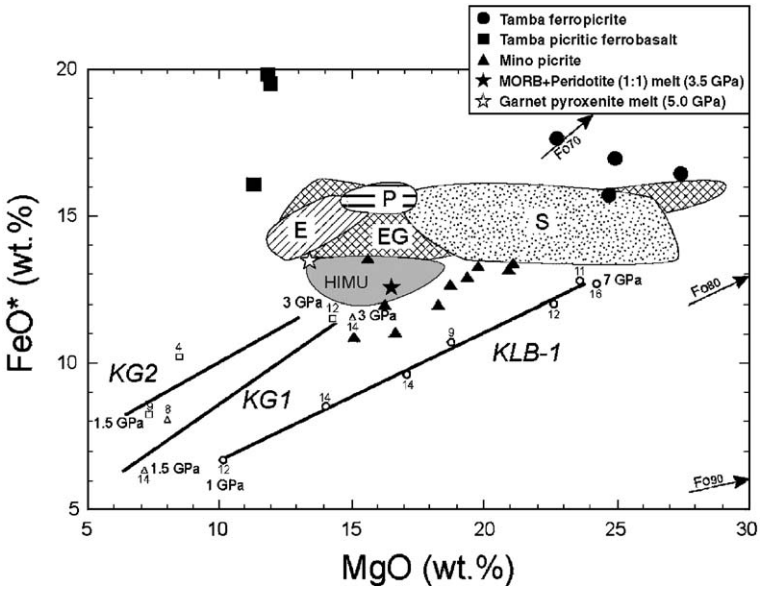

Fig. 10. The FeO*–MgO relationships between the Tamba ferropicrite and picritic ferrobasalt and the melting experimental results. The representative terrestrial ferropicrites (E=Etendeka, EG=East Greenland, P=Pechenga, S=Siberia; references are shown in caption of Fig. 4) and HIMU-type picrites (Kogiso et al., 1997) are also shown. The compositions of melt from KLB-1 (circle) are after Hirose and Kushiro (1993) and Walter (1998). Those from KG1 (KLB-1/MORB=2:1; triangle) and KG2 (KLB-1/MORB=1:1; square) are after Kogiso et al. (1998). The numbers near the plots indicate degree of partial melting. The black star shows the melt composition (at 1500 °C and 3.5 GPa) from the mixed MORB (GA1) and MORB pyrolite (MPY90) by Yaxley and Green (1998). The open star shows the melt composition (at 1650 °C and 5.0 GPa) from garnet pyroxenite by Kogiso et al. (2003). The arrows indicate the lines tying olivine with variable composition and the origin.

picrite is plotted near HIMU fields, and the other ferropicrites extend into EMI–EMII direction along low $\varepsilon Nd_{(i)}$ side of mantle array. This indicates that their sources consist of the variable proportion of the mixture of HIMU and EM, and involved pelagic sediments in addition to subducted oceanic crust (e.g. Dostal et al., 1998). In the previous studies for ferropicrite genesis, Walker et al. (1997) examined Re–Os isotope of the Proterozoic ferropicrites from Pechenga, and revealed that the ferropicrite was originated from the plume mantle source with large proportions of recycled oceanic crust. Gibson (2002) suggested that the iron-rich picritic melt is produced by the partial melting of basalt+peridotite mixture at ≧1450 °C and ≧4.5 GPa. Arndt et al. (1998) and Arndt (2003) also interpreted that the meimechite associated with the Siberian ferropicrite was produced by the low degree (2%) of partial melting of MORB+peridotite at great depth (>6–7 GPa).

As mentioned above, the unusual iron-rich nature of the Tamba ferropicrite and picritic ferrobasalt cannot be explained by crystal fractionation from a parental magma with an ordinary iron content. In the melting experiments of primitive (pyrolitic) mantle, the iron content of partial melts is sensitive to the change of pressure rather than the degree of partial melting, and increases with increasing pressure (e.g. Hirose and Kushiro, 1993; Walter, 1998). The melt compositions obtained by the melting experiments of the various materials are shown in Fig. 10. The melt compositions in this diagram are of the lowest degree of partial melting at each melting pressure (<16%), because the ferropicrites used in this study appear to have been produced by relatively low degrees of melting (Fig. 8). If the mantle source was pyrolitic, the Tamba ferropicrite and picritic ferrobasalt require surprisingly deep melt segregation depth (>7 GPa), which is inconsistent with the estimated pressure in $Zr/Y-TiO_2/Al_2O_3$ diagram (Fig. 9). The HIMU-type basalt trends to be more enriched in iron than other OIBs (e.g. Kogiso et al., 1997), and it is likely that the involvement of subducted oceanic crust in the mantle source region can produce iron-rich partial melt. This is confirmed by the melting experiment of the mixture of MORB+peridotite, which results in higher iron content than that of primitive mantle (Kogiso et al., 1998). Therefore, the involvement of subducted oceanic crust component may play a very important role in the genesis of ferropicrite. However, the unusually high FeO* content up to 20 wt.% of the Tamba picritic ferrobasalt requires more MORB component than 50% on the basis of the melting experiment of the mixture of MORB+peridotite, but the partial melting of such source material can no longer produce iron-rich magnesian melt. Terrestrial ferropicrites more or less contain igneous hydrous phases such as phlogopite and kaersutite as phenocryst and/or groundmass minerals. This means that the source material of ferropicrite commonly contains H_2O. However, the melts from the melting experiment of hydrous peridotite show lower FeO* content than those of dry peridotite (Kawamoto and Holloway, 1997). It is unlikely that the iron-rich nature of ferropicrite is due to melting of a wet mantle material (Gibson, 2002). The recycling of ferromanganese crusts and nodules with oceanic crust into mantle (Baker and Jensen, 2004) can produce the iron-rich picritic melt. Nevertheless, much amount of ferromanganese material not only make the picritic melt richer in iron but also make it highly manganiferous and very high in Sr isotopic ratio. The latter features have never been observed among the ferropicrites.

The most reasonable explanation for the genesis of ferropicrite is the melting of the recycled iron- (and titanium-) rich basalt and/or gabbro. It is known that the occurrence of iron-rich basalt, gabbro and glass (up to 20 wt.% in FeO*) are widespread in ocean floor such as East Pacific Rise, Indian Ridge and Galapagos Ridge (e.g. Regelous et al., 1999; Embley et al., 1988; Coogan et al., 2001). In addition, the iron-rich (~20 wt.% in FeO*) eclogite with evolved MORB chemistry also occurs in some peridotite massifs (e.g. the Voltri massif, Alps: Mottana and Bocchio, 1975; Ernst et al., 1983), and this indicates that iron-rich MORBs were actually subducted to the deeper mantle. The involvement of the iron-rich MORB can produce the unusual high-FeO* picritic melt without significant modification of HIMU isotopic characteristics. Fig. 8 shows the compositional path of the melts from the mixture of primitive mantle+Fe-rich eclogite (Fe-rich basalt). The path is placed to the right of another path for a mixture of peridotite+eclogite (MORB), which indicate that the melts produced by the melting of peridotite+Fe-rich eclogite (basalt) are more enriched in Zr at a given degree of partial melting. The picritic ferrobasalts are plotted between the two compositional paths, fitting to our modeling. If the recycled oceanic crust is Fe-rich gabbroic rock that is poorer in trace elements, the compositional path should have shifted more to the left. The Fe-rich gabbros from the ocean floor show the positive Ti anomaly (e.g. Coogan et al., 2001), and the positive anomaly of Ti observed in the picritic ferrobasalt and some other ferropicrites (Fig. 5) would have been inherited from the Fe, Ti-rich gabbro.

The genesis of the Tamba ferropicrite is ambiguous, because its high MgO content requires the partial melting at a high pressure (possibly up to 7 GPa; Fig. 10) even if the subducted oceanic crust was involved in its source region. This is inconsistent with the shallower melt segregation depth than that of the picritic ferrobasalt and Mino picrite, because these rocks and the ferropicrite show the same Nb/Zr and initial isotopic ratio. The high MgO content of the ferropicrite would have resulted from olivine accumulation. This is consistent with the petrographic observations that the ferropicrite shows phyric and poikilitic texture, and contains abundant olivine and clinopyroxene. In this case, if a half of the olivine phenocrysts in the ferropicrite (20 vol.%) is accumulated crystals, assuming average Fo_{78} composition (approximately MgO=40 wt.% and FeO=20 wt.%), the increase of 4 wt.% in FeO* results from the accumulation. However, the size of the olivine phenocryst in the ferropicrite is commonly <1 mm, and it is unlikely that the accumulation of a large amount of olivine took place in the ferropicrite. Additionally, the possible accumulation of olivine+clinopyroxene causes less important increase FeO* than pure olivine accumulation. Therefore, it seems that the parental magma of the ferropicrite would also have contained higher FeO*, and that the recycling of iron-rich MORB into mantle source region should be required.

Although peridotites, pyroxenites and peridotite/eclogite (MORB) mixtures have ever been experimentally molten to determine the composition of partial melts, any of the starting materials, except for the Martian mantle enriched in iron (Bertka and Holloway, 1994), cannot produce the melts with the composition comparable to terrestrial ferropicrites, especially the Tamba ferropicrite. Our model is essentially consistent with the previous ideas that the source mantle of ferropicrite may contain subducted ancient oceanic crust, but we prefer the recycling of the Fe-rich basalt with evolved MORB composition to produce the ferropicritic melt.

6.5. Geodynamic implication of the ferropicrite

The geological, petrological and isotopic evidences clearly indicate that the Tamba ferropicritic rocks were derived from the Permian oceanic mantle plume. Ferropicrites are rare in Phanerozoic. Gibson (2002) emphasized that ferropicrite occurs at basal part of a thick volcanic sequence, and it is a consequence of the melting of the margin of a mantle plume head. However, the Tamba ferropicritic rocks clearly intruded into more voluminous basaltic rocks, suggesting that they formed after the main basaltic volcanic activities. The ferropicrites from Siberia and East Greenland also appear as dikes and lavas later than the eruption of voluminous continental flood basalt (Arndt et al., 1995; Peate et al., 2003). These ferropicrites also have compositional characteristics indicating the low degrees of partial melting (Fig. 8). This suggests that a colder mantle plume tail with recycled oceanic crust can melt to produce ferropicrite after the arrival of a hotter mantle plume head.

It has been suggested that most mafic volcanic rocks in the Mino–Tamba accretionary complex represent remnants of many seamounts or oceanic islands in the paleo-Pacific ocean in Carboniferous to Permian. Sano and Tazaki (1989) and Sano et al. (2000) studied the greenstones from the Tamba belt, and concluded that the greenstones were derived from the ocean islands composed of tholeiitic and alkali basalt and from the ocean floor composed of N-MORB. Jones et al. (1993) suggested that the tholeiitic volcanic rocks compositionally equivalent to E-MORB from the Funafuseyama area, Mino belt were originated from axis-centered oceanic plateau with a bathymetrically elevated feature like Iceland on the basis of their chemical composition and association with huge limestone reefs.

It is difficult to decipher the original volcanic edifices of the greenstones from their fragmental occurrences among the accretionary complexes. However, the occurrence of relatively rare volcanic rocks such as ferropicrite may help us to understand the origin of the greenstones and the ancient oceanic magmatism. The plume-related ocean island basalt is mainly alkalic and is associated with fractionated rocks such as phonolite and trachyte, while the greenstones from the Mino–Tamba belt are dominated by tholeiitic to alkaline basalt, and the fractionated rocks are very rare. In most LIPs, tholeiitic to alkalic basalts are also dominant. Ontong Java plateau mainly consists of tholeiitic basalt, but HIMU-like ferromagnesian basalts (MgO=11 wt.% and FeO*=14 wt.% in anhydrous) are also reported (Tejada et al., 1996). Gibson (2002) reviewed the occurrence of terrestrial ferropicrites from Archean to Phanerozoic, and indicated that they typically occur in LIPs. Ichiyama and Ishiwatari (2005) pointed out that HFSE-rich picrites, including the Mino picrite, typically occur in superplume region, and that the presence of the Mino HFSE-rich picrite indicates that the basaltic rocks in the Mino belt would be produced by the upwelling of Permian superplume. The occurrence of the ferropicrite and picritic ferrobasalt of the Permian age in the Jurassic Mino–Tamba accretionary complex indicates a possibility that the

Mino–Tamba accretionary complex includes many fragments of a Permian LIP that accreted into the subduction zone in the Jurassic time. The ancient oceanic plateaux accreted to continental margin or arc have been recognized in some accretionary complexes (Wrangellia terrane, North America: Lassiter et al., 1995; Sorachi-Yezo belt, Japan: Kimura et al., 1994; Tatsumi et al., 1998; Nagahashi and Miyashita, 2002), and parts of the present-day Ontong Java and Caribbean plateaux indeed are obducted to Solomon Islands (e.g. Tejada et al., 1996) and South America (e.g. Kerr et al., 1997), respectively. If so, the greenstones of the Mino–Tamba accretionary complex would have been an oceanic plateau formed in paleo-Pacific ocean, which may be a new Late Paleozoic LIP other than the two known Permian continental flood basalt provinces (Siberia, Russia, and Emeishan, China). More detailed petrological and geochemical studies are required to understand geodynamics of the Permian oceans.

7. Conclusion

(1) The Permian ferropicritic rocks occur in the Mino–Tamba belt as dikes intruded into the mafic rocks. They are characterized by high MgO, FeO* and HFSE contents, and the mineralogical evidence indicates that their unusual iron-rich nature is of magmatic origin.

(2) The incompatible element contents and ratios indicate that the picritic ferrobasalt has strong genetic kinship with the highly HFSE-rich Mino picrite, and they were produced by the low degree of partial melting of HFSE-enriched source material at a high pressure. On the other hand, the Tamba ferropicrite was produced by the same degree of partial melting at a lower pressure, and would be affected by olivine accumulation. The Sr and Nd isotopic signatures of the Tamba ferropicritic rocks and the Mino picrite are nearly homogeneous and indicate HIMU source. Nevertheless, the Tamba ferropicritic rocks cannot be fractionated from the Mino picrite.

(3) To produce the unusually iron-rich picritic melt, unreasonable addition of basaltic component or partial melting at unexpectedly high pressure is required. The most reasonable source material of the ferropicrite is the mixture of recycled Fe- and Ti-rich basalt (and/or gabbro) and mantle peridotite. Such a ferrobasalt and its metamorphosed equivalent occur in the present ocean floor and in some peridotite massifs as Fe- and Ti-rich eclogite, respectively.

(4) The Tamba ferropicritic rocks were derived from the Permian mantle plume in an oceanic setting, and may have formed after the arrival of its plume head. The plural occurrences of the ferropicritic rocks and HFSE-rich picrite from the Mino–Tamba accretionary complex imply that this accretionary complex would be fragments of an oceanic plateau formed by the Permian superplume activities on paleo-Pacific ocean, and was subsequently accreted to the continental margin by subduction in the Jurassic time.

Acknowledgements

We thank S. Arai and T. Morishita of Kanazawa University for several discussions. We are grateful for constructive reviews by two anonymous reviewers. We thank J. Takada and K. Takamiya of the Kyoto University Research Reactor Institute and T. Nakanishi, Y. Nagamura, K. Washiyama and R. Amano of Kanazawa University for their help for INAA analysis. K. Koizumi is thanked for the assistance in the fieldwork. M. Shirasaka and Y. Shimizu also are thanked for the assistance of ICP–MS and EPMA analysis, respectively. We also acknowledge that the Master thesis of T. Muto (2001) of Kanazawa University inspired our research in the Obama area.

References

Arai, S., 1992. Chemistry of chromian spinel in volcanic rocks as a potential guide to magma chemistry. Mineral. Mag. 56, 173–184.

Arndt, N., 2003. Komatiite, kimberlite, and boninite. J. Geophys. Res. 108B6, 2293.

Arndt, N., Lehnert, K., Vasil'ev, Y., 1995. Meimechites: highly magnesian alkaline magmas from the subcontinental lithosphere? Lithos 34, 41–59.

Arndt, N., Chauvel, C., Czamanske, G., Fedorenko, V., 1998. Two mantle sources, two plumbing systems: tholeiitic and alkaline magmatism of the Maymecha River basin, Siberian flood volcanic province. Contrib. Mineral. Petrol. 133, 297–313.

Baker, J.A., Jensen, K.K., 2004. Cupled ^{186}Os–^{187}Os enrichments in the Earth's mantle–core–mantle interaction or recycling of ferromanganese crusts and nodules? Earth Planet. Sci. Lett. 220, 277–286.

Bertka, C.M., Holloway, J.R., 1994. Anhydrous partial melting of an iron-rich mantle: II. Primary melt compositions at 15 kbar. Contrib. Mineral. Petrol. 115, 323–338.

Chaffey, D.J., Cliff, R.A., Wilson, B.M., 1989. Characterization of the St. Helena magma source. In: Saunders, A.D., Norry, M.J. (Eds.), Magmatism in the Ocean Basins. Geol. Soc. Spec. Publ. vol. 42, pp. 257–276.

Chauvel, C., Hofmann, A.W., Vidal, P., 1992. HIMU-EM: the French Polynesian connection. Earth Planet. Sci. Lett. 110, 99–119.

Coogan, L.A., MacLeod, C.J., Dick, H.J.B., Edwards, S.J., Kvassnes, A., Natland, J.H., Robinson, P.T., Tompson, G., O'Hara, M.J.,

2001. Whole-rock geochemistry of gabbros from the Southwest Indian Ridge: constraints on geochemical fractionations between the upper and lower oceanic crust and magma chamber processes at (very) slow-spreading ridges. Chem. Geol. 178, 1–22.

Dick, H.J.B., Bullen, T., 1984. Chromium spinel as a petrogenetic indicator in abyssal and alpine-type peridotites and spatially associated lavas. Contrib. Mineral. Petrol. 86, 54–76.

Dostal, J., Cousens, B., Dupuy, C., 1998. The incompatible characteristics of an ancient subducted sedimentary component in oceanic island basalts from French Polynesia. J. Petrol. 39, 937–952.

Embley, R.W., Jonasson, I.R., Perfit, M.R., Franklin, J.M., Tivey, M.A., Malahoff, A., Smith, M.F., Francis, T.J.G., 1988. Submersible investigation of an extinct hydrothermal system on the Galapagos Ridge: sulfide mound, stockwork zone, and differentiated lavas. Can. Mineral. 26, 517–539.

Ernst, W.G., Rambaldi, E., Piccardo, G.B., 1983. Trace element geochemistry of iron+titanium-rich eclogitic rocks, Gruppo di Voltri, western Liguria. J. Geol. 91, 413–425.

Francis, D., Ludden, J., Johnstone, R., Davis, W., 1999. Picrite evidence for more Fe in Archean mantle reservoirs. Earth Planet. Sci. Lett. 167, 197–213.

Gibson, S.A., 2002. Major element heterogeneity in Archean to recent mantle plume starting-heads. Earth Planet. Sci. Lett. 195, 59–74.

Gibson, S.A., Thompson, R.N., Dickin, A.P., 2000. Ferropicrites: geochemical evidence for Fe-rich streaks in upwelling mantle plumes. Earth Planet. Sci. Lett. 174, 355–374.

Halliday, A.N., Lee, D.C., Tommasini, S., Davies, G.R., Paslick, C.R., Fitton, J.G., James, D.E., 1995. Incompatible trace elements in OIB and MORB and source enrichment in the sub-oceanic mantle. Earth Planet. Sci. Lett. 133, 379–395.

Hanski, E.J., 1992. Petrology of the Pechenga ferropicrites and cogenetic, Ni-bearing gabbro–wehrlite intrusions, Kola Peninsula, Russia. Geol. Surv. Finl., Bull. 367, 192.

Hanski, E.J., Smolkin, V.F., 1989. Pechenga ferropicrites and other early Proterozoic picrites in the eastern part of the Baltic Shield. Precambrian Res. 45, 63–82.

Hanski, E.J., Smolkin, V.F., 1995. Iron- and LREE-enriched mantle source for early Proterozoic intraplate magmatism as exemplified by the Pechenga ferropicrites, Kola Peninsula, Russia. Lithos 34, 107–125.

Hanski, E.J., Huhma, H., Smolkin, V.F., 1990. The age of the ferropicritic volcanics and comagmatic Ni-bearing intrusions at Pechenga, Kola Peninsula. USSR Bull. Geol. Soc. Finland 62, 123–133.

Hirose, K., Kushiro, I., 1993. Partial melting of dry peridotites at high pressures: determination of compositions of melts segregated from peridotite using aggregates of diamond. Earth Planet. Sci. Lett. 114, 477–489.

Hofmann, A.W., 1988. Chemical differentiation of the Earth: the relationship between mantle, continental crust, and oceanic crust. Earth Planet. Sci. Lett. 90, 297–314.

Ichiyama, Y., Ishiwatari, A., 2005. HFSE-rich picritic rocks from the Mino accretionary complex, southwestern Japan. Contrib. Mineral. Petrol. 149, 373–387.

Ishida, T., Arai, S., Takahashi, N., 1990. Metamorphosed picrite basalts in the northern part of the Setogawa belt, central Japan. J. Geol. Soc. Jpn. 96, 181–191 (in Japanese with English abstract).

Ishiwatari, A., Tsujimori, T., 2003. Paleozoic ophiolites and blueschists in Japan and Russian Primorye in the tectonic framework of East Asia: a synthesis. Isl. Arc 12, 190–206.

Ishiwatari, A., Ichiyama, Y., 2004. Alaskan-type plutons and ultramafic lavas in Far East Russia, Northeast China and Japan. Int. Geol. Rev. 46, 316–331.

Isomi, H., Kuroda, K., 1958. Geology of the western part of Wakasa Direct, Fukui Prefecture: with phrticular reference to the structure and stratigraphy of Permian. Bull. Geol. Surv. Jpn. 9, 133–143 (in Japanese with English abstract).

Isozaki, Y., 1997. Jurassic accretion tectonics of Japan. Isl. Arc 6, 25–51.

Isozaki, Y., Maruyama, S., 1991. Studies on orogeny based on plate tectonics in Japan and new geotectonic subdivision of the Japanese islands. J. Geogr. 100, 697–761 (in Japanese with English abstract).

Jones, G., Valsami-Jones, E., Sano, H., 1993. Nature and tectonic setting of accreted basalts from the Mino terrane, central Japan. J. Geol. Soc. (Lond.) 150, 1167–1181.

Kawamoto, T., Holloway, J.R., 1997. Melting temperature and partial melt chemistry of H_2O-saturated mantle peridotite to 11 gigapascals. Science 276, 240–243.

Kerr, A.C., Tarney, J., Marriner, G.F., Nivia, A., Saunders, A.D., 1997. The Caribbean–Colombian Cretaceous igneous province: the internal anatomy of an oceanic plateau. In: Mahoney, J.J., Coffin, M. (Eds.), Large Igneous Provinces; Continental, Oceanic and Planetary Flood Volcanism. Geophys. Monogr., vol. 100, pp. 45–93.

Kimura, G., Sakakibara, M., Okamura, M., 1994. Plumes in central Panthalassa? Deductions from accreted oceanic fragments in Japan. Tectonics 13, 905–916.

Kogiso, T., Tatsumi, Y., Shimoda, G., Barsczus, H.G., 1997. High μ (HIMU) ocean island basalts in southern Polynesia: New evidence for whole mantle scale recycling subducted oceanic crust. J. Geophys. Res. 102, 8085–8103.

Kogiso, T., Hirose, K., Takahashi, E., 1998. Melting experiments on homogeneous mixtures of peridotite and basalt: application to the genesis of ocean island basalts. Earth Planet. Sci. Lett. 162, 45–61.

Kogiso, T., Hirschmann, M.M., Frost, D.J., 2003. High-pressure partial melting of garnet pyroxenite: possible mafic lithologies in the source of oceanic islands basalts. Earth Planet. Sci. Lett. 216, 603–617.

Lassiter, J.C., DePalo, D.J., Mahoney, J.J., 1995. Geochemistry of the Wrangellia flood basalt province: implications for the role of continental and oceanic lithosphere in flood basalt genesis. J. Petrol. 36, 983–1009.

Le Roex, A.P., Cliff, R.A., Adair, B.J.I., 1990. Tristan da Cunha South Atlantic: geochemistry and petrogenesis of a basanite–phonolite lava series. J. Petrol. 31, 779–812.

Loucks, R.R., 1996. A precise olivine–augite Mg–Fe-exchange geothermometer. Contrib. Mineral. Petrol. 125, 140–150.

Miyazaki, T., Shuto, K., 1998. Sr and Nd isotope ratios of twelve GSJ rock reference samples. Geochem. J. 32, 345–350.

Mottana, A., Bocchio, R., 1975. Superferric eclogite of the Voltri Group (Pennidic belt, Apennines). Contrib. Mineral. Petrol. 49, 201–210.

Nagahashi, T., Miyashita, S., 2002. Petrology of the greenstones of the Lower Sorachi Group in the Sorach–Yezo Belt, central Hokkaido, Japan, with special reference to discrimination between oceanic plateau basalts and mid-oceanic ridge baalts. Isl. Arc 11, 122–141.

Nakae, S., 2000. Regional correlation of the Jurassic accretionary complex in the inner zone of southwest Japan. Mem. Geol. Soc. Jpn. 55, 73–98 (in Japanese with English abstract).

Nakae, S., Yoshioka, T., 1998. Geology of Kumagawa district. With geological sheet map at 1:50,000. Geol. Surv. Japan, 71P (in Japanese with English abstract).

Nicholls, J., Stout, M.Z., 1988. Picritic melts in Kilauea — evidence from the 1967–1968 Halemaumau and Hiiaka eruptions. J. Petrol. 29, 1031–1057.

Norman, M.D., Garcia, M.O., 1999. Primitive magmas and source characteristics of the Hawaiian plume: petrology and geochemistry of shield picrites. Earth Planet. Sci. Lett. 168, 27–44.

Peate, D.W., Baker, J.A., Blichert-Toft, J., Hilton, D.R., Storey, M., Kent, A.J.R., Brooks, C.K., Hansen, H., Pedersen, A.K., Duncan, R.A., 2003. The Prinsen af Wales Bjerge Formation Lavas, East Greenland: the transition from tholeiitic to alkalic magmatism during Palaeogene continental break-up. J. Petrol. 44, 279–304.

Regelous, M., Niu, Y., Wendt, J.I., Batiza, R., Greig, A., Collerson, K.D., 1999. Variations in the geochemistry of magmatism on the East Pacific Rise at 10°30′N since 800 ka. Earth Planet. Sci. Lett. 168, 45–63.

Roeder, P.L., Emslie, R.F., 1970. Olivine–liquid equilibrium. Contrib. Mineral. Petrol. 29, 275–289.

Sack, R.O., Walker, D., Carmichael, I.S.E., 1987. Experimental petrology of alkalic lavas: constraints on cotectics of multiple saturation in natural basic liquids. Contrib. Mineral. Petrol. 96, 1–23.

Sakaguchi, S., Hasegawa, T., Morimoto, K., 1973. Geology of the Obama Area, Fukui prefecture. Mem. Osaka Kyoiku Univ. 22, 55–67 (in Japanese with English abstract).

Sano, S., Tazaki, K., 1989. Greenstones in the Tamba belt. Mem. Geol. Soc. Jpn. 33, 53–67. (in Japanese with English abstract).

Sano, S., Hayasaka, Y., Tazaki, K., 2000. Geochemical characteristics of Carboniferous greenstones in the inner zone of southwest Japan. Isl. Arc 9, 81–96.

Shaw, D.M., 1970. Trace element fractionation during anatexis. Geochim. Cosmochim. Acta 34, 237–243.

Shirasaka, M., Arai, S., Ishimaru, S., Ishida, Y., Shimizu, Y., Morishita, T., 2004. The solution introduction ICP–MS technique to trace element analysis of rocks. Sci. Rep. Kanazawa Univ. 48, 43–71.

Sigurdsson, I.A., Steinthorsson, S., Grönvold, K., 2000. Calcium-rich melt inclusions in Cr-spinels from Borgarhraun, northern Iceland. Earth Planet. Sci. Lett. 183, 15–26.

Skovgaard, A.C., Storey, M., Baker, J.A., Blusztajn, J., 2001. Osmium–oxygen isotopic evidence for a recycled and strongly depleted component in the Iceland mantle plume. Earth Planet. Sci. Lett. 194, 259–275.

Stille, P., Unruh, D.M., Tatsumoto, M., 1986. Pb, Sr, Nd, and Hf isotopic constrains on the Hawaiian basalts and evidence for a unique mantle source. Geochim. Cosmochim. Acta 50, 2303–2319.

Sun, S.S., McDonough, W.F., 1989. Chemical and isotopic systematics of oceanic basalts: implications for mantle composition and processes. In: Saunders, A.D., Norry, M.J. (Eds.), Magmatism in the Ocean Basins. Geol. Soc. Spec. Publ. vol. 42, pp. 313–345.

Tatsumi, Y., Shinjoe, H., Ishizuka, H., Sager, W.W., Klaus, A., 1998. Geochemical evidence for a mid-Cretaceous superplume. Geology 26, 151–154.

Tejada, M.L.G., Mahoney, J.J., Duncan, R.A., Hawkins, M.P., 1996. Age and geochemistry of basement and alkali rocks of Malaita and Santa Isabel, Solomon Islands, southern margin of Ontong Java Plateau. J. Petrol. 37, 361–394.

Wakita, K., 1988. Origin of chaotically mixed rock bodies in the Early Jurassic to Early Cretaceous sedimentary complex of the Mino terrane, central Japan. Bull. Geol. Surv. Jpn. 39, 675–757.

Walker, R.J., Morgan, J.W., Hanski, E.J., Smolkin, V.F., 1997. Re–Os systematics of Early Proterozoic ferropicrites, Pechenga Complex, northern Russia: for ancient ^{187}Os-enriched plumes. Geochim. Cosmochim. Acta 61, 3145–3160.

Walter, M.J., 1998. Melting of garnet peridotite and the origin of komatiite and depleted lithosphere. J. Petrol. 39, 29–60.

Weaver, B.L., 1991. The origin of oceanic island basalt end-member compositions: trace element and isotopic constraints. Earth Planet. Sci. Lett. 104, 115–118.

White, W.M., Hofmann, A.W., Puchelt, H., 1987. Isotope geochemistry of Pacific mid-ocean ridge basalts. J. Geophys. Res. 92, 4881–4893.

Wright, E., White, W., 1987. The origin of Samoa: new evidence from Sr, Nd and Pb isotopes. Earth Planet. Sci. Lett. 81, 151–162.

Yaxley, G.M., Green, D.H., 1998. Reactions between eclogite and peridotite: mantle refertilisation by subduction of oceanic crust. Schweiz. Mineral. Petrogr. Mitt. 78, 243–255.

Zindler, A., Hart, S., 1986. Chemical geodynamics. Annu. Rev. Earth Planet. Sci. 14, 493–571.